STAMP-Based Digital CRISPR-Cas13a (STAMP-dCRISPR) for Amplification-Free Quantification of HIV-1 Plasma Viral Loads

Reza Nouri [1], Yuqian Jiang [2], Anthony J. Politza [2], Tianyi Liu [1], Wallace H. Greene [3], Yusheng Zhu [3], Jonathan J. Nunez [4], Xiaojun Lian [2,5,6] and Weihua Guan [1, 2, *]

[1] Department of Electrical Engineering, Pennsylvania State University, University Park, Pennsylvania 16802, United States

[2] Department of Biomedical Engineering, Pennsylvania State University, University Park, Pennsylvania 16802, United States

[3]Department of Pathology, Penn State College of Medicine, Hershey, PA 17033, United States

[4] Department of Medicine, Penn State College of Medicine and Milton S. Hershey Medical Center, Hershey, Pennsylvania 17033, United States

[5] Huck Institutes of the Life Sciences, Pennsylvania State University, University Park, Pennsylvania 16802, United States

[6] Department of Biology, Pennsylvania State University, University Park, Pennsylvania 16802, United States

* Correspondence should be addressed to wzg111@psu.edu

ABSTRACT

Quantification of HIV RNA in plasma is critical for identifying the disease progression and monitoring the effectiveness of antiretroviral therapy. While RT-qPCR has been the gold standard for HIV viral load quantification, digital assays could provide an alternative calibration-free absolute quantification method. Here, we reported a Self-digitization Through Automated Membrane-based Partitioning (STAMP) method to digitalize the CRISPR-Cas13 assay (dCRISPR) for amplification-free and absolute quantification of HIV-1 viral RNAs. The HIV-1 Cas13 assay was designed, validated, and optimized. We evaluated the analytical performances with synthetic RNAs. With a membrane that partitions ~100 nL reaction mixture (containing effective 10 nL input RNA sample), we showed that RNA samples spanning 4 orders of dynamic range between 1 fM (~6 RNAs) to 10 pM (~60k RNAs) could be quantified as fast as 30 min. We also examined the end-to-end performances from RNA extraction to STAMP-dCRISPR quantification using 140 μL of both spiked and clinical plasma samples. We demonstrated that the device has a detection limit of approximately 2000 copies/ml and can resolve a viral load change of 3571 copies/ml (equivalent to 3 RNAs in a single membrane) with 90% confidence. Finally, we evaluated the device using 140 μL of 20 patient plasma samples (10 positives and 10 negatives) and benchmarked the performance with RT-PCR. The STAMP-dCRISPR results agree very well with RT-PCR for all negative and high positive samples with C_t<32. However, the STAMP-dCRISPR is limited in detecting low positive samples with C_t>32 due to the subsampling errors. Our results demonstrated a digital Cas13 platform that could offer an accessible amplification-free quantification of viral RNAs. By further addressing the subsampling issue with approaches such as preconcentration, this platform could be further exploited for quantitatively determining viral load for an array of infectious diseases.

KEYWORDS

CRISPR, Cas 13a, HIV-1, Digital, Viral load, Quantification

Acquired immunodeficiency syndrome (AIDS) caused by human immunodeficiency virus (HIV) infection, a notorious fatal epidemic, has led to millions of deaths worldwide since its origin [1]. Although AIDS-related annual mortality has reduced by 33% in the past decade due to the application of antiretroviral therapies and advanced HIV diagnosis, the number of new HIV infections remains high (for instance, 1.5 million in 2020 globally), which is estimated to cost billions of dollars for AIDS therapy [2]. Since AIDS patients at early stages tend to present no obvious symptoms but can still be infectious, early awareness of infection enables timely treatment for exposed patients and prevents further transmission [3]. Viral load monitoring of the HIV-1 RNA not only identifies the progression of the disease in a patient but also could be employed to monitor the effectiveness of antiretroviral therapy and the trends in large populations of patients [4-6]. So far, nucleic acid tests (NAT) hold tremendous promise in viral load testing [7]. One of the major techniques for viral load quantification of HIV is the reverse transcriptase quantitative polymerase chain reaction (RT-qPCR) due to its accessibility and high sensitivity [4, 8-10]. Although RT-qPCR has been the gold standard for detecting the HIV-1 RNA, the emerging clustered regularly interspaced short palindromic repeats (CRISPR) based technology has taken immense attention for nucleic acid tests due to its high sensitivity and specificity [11-12].

Since the discovery of Cas9 proteins for gene editing, CRISPR technology has taken center stage in biotechnology [13]. Recently, the discovery of the collateral cleavage in other Cas proteins like Cas12 [14] and Cas13 [15] made it possible to translate the sequence-specific targeting to other detectable signals, which has led to the increasing emergence of CRISPR-mediated biosensors [15-28]. Among these CRISPR-mediated assays, a preamplification step is often required to boost the limit of detection (LOD) and time to results performance [23, 29]. However, preamplification complicates the assay setup, increases the assay time, raises the risk of contamination, and could introduce false-negative or -positive results due to amplification errors [30]. We previously surveyed different strategies in the literature to boost the CRISPR assay performance [31], such as the use of Cas proteins with higher cleavage activity [32], the use of multiple crRNA in the reaction [33-34], the use of a sensitive readout system [35], and the reaction digitization [34, 36-47]. Among these techniques, we found only the digitization method could match the LOD (attomolar range) and the fast turnaround time (less than 1 hour) of preamplification-coupled CRISPR assays [31].

So far, various digitization techniques have been introduced. For instance, water in oil droplets generated by T-junction [48], flow focusing [49-50], and centrifugation [51] have been used for

digitization. Furthermore, digital assays have been performed inside numerous microchambers fabricated by polydimethylsiloxane (PDMS) or glass chambers. Partitioning of the assay inside these chambers has been achieved using vacuum [52-53], pressure [54], SlipChip [55], hydrophilic patterns [56-57], or self-digitization [58]. Often complicated fluidic control systems and complex micro and nanofabrication processes are required. There are recent research efforts to simplify the digitization process. For instance, a real-time digital loop-mediated isothermal amplification (LAMP) was performed using commercially available microfluidic chips by Rolando *et al.* [59]. In another study, Lin *et al*. utilized a commercial membrane for LAMP assay digitization without the need for complex chip fabrication or use of specialized equipment [60-61].

In this study, we reported a Self-digitization method Through Automated Membrane-based Partitioning (STAMP) and developed a STAMP-based digital CRISPR-Cas13a (STAMP-dCRISPR) for the absolute quantification of HIV-1 viral load. We first established and characterized the STAMP method to digitalize the reaction inside a track-etched polycarbonate (PCTE) membrane. We then designed, validated, and optimized the HIV-1 Cas13 assay by evaluating different CRISPR RNA (crRNA) designs and their catalytic efficiency on the sensing performance. The analytical limit of detection and the dynamic range of the STAMP-dCRISPR was evaluated by synthetic HIV-1 RNAs. Finally, we evaluated the end-to-end performances from RNA extraction to STAMP-dCRISPR quantification using 140 µL of contrived and clinical plasma samples to examine the viral load resolution and the clinical applicability of the proposed method.

RESULTS

STAMP digitization and characterization

To achieve self-digitization without complicated fluidic control, we developed the STAMP to digitalize the assay (See Methods for details). In this method, a commercial polycarbonate track-etched (PCTE) membrane was utilized for digitization. This type of membrane consists of a high density of pores with uniform sizes ranging from 10 nm to 30 µm [60]. **Figure 1a** illustrates a top and side view of the assembled STAMP where the membrane of a diameter of 1.3 cm is sandwiched between a polymethyl methacrylate (PMMA) holder and a thin tape (70 µm thickness). **Figure 1b** shows the pore characterization results from 5 different membranes. The average pore size was measured as 24.6±1.6 µm, and the pore density was determined to be

9895±531 pores/cm^2.

The operation of the STAMP only requires 4 simple manual steps (**Video S1**). In the first step (**Figure 1c-i**), the analyte sample droplet was deposited on top of a glass surface, and the device was slowly placed on top of it. Only 8 μL of the sample was required to ensure the filling process, which is 33% more than the spacing volume of 6 μL between the membrane and glass surface. Once in contact, the surface tension between the sample and pore walls causes a capillary action that forces the sample into the membrane's pores. After 60 seconds of soaking, 60 μL of mineral oil was added to the top chamber to seal the top surface of the membrane (**Figure 1c-ii**). An inspection of the STAMP confirmed that all pores were successfully filled even though there were excessive liquids underneath the membrane (**Figure S1a**). To remove these excessive samples, one only needs to peel off the STAMP from the glass surface (**Figure 1c-iii**). The as-purchased membranes were coated with polyvinylpyrrolidone (PVP) which renders the surface hydrophilic. This hydrophilic coating was removed by dipping the membranes in 10% acetic acid for 30 minutes and heating them at 140 °C for 60 minutes in a vacuum oven to facilitate the excessive liquid removal. **Figure 1d** shows that the contact angle increased from 48 to 79 degrees after this chemical treatment, confirming the PVP removal process. Since the contact angle of the glass surface is much lower than that of the treated PCTE membrane surface, the excess liquid would remain on the glass and be removed from the PCTE membrane surface. In the pore areas, the surface tension overcomes the liquid intermolecular forces and holds the sample inside the pores. An examination of the STAMP confirms this process for effectively removing the excess liquid while maintaining the digitalized samples (**Figure S1b**). Lastly, the STAMP was placed on top of a customized base with prefilled mineral oil (**Figure 1c-iv**) to form a fully sealed digital system for further reaction. It is worth noting that each STAMP would accommodate ~100 nL of liquid on the membrane for digitization.

To evaluate the membrane filling process and evaporation under heating procedures, we measured the filling ratio (total number of filled pores per total number of pores) of the final sealed membrane before and after 30 minutes of heating at 37 °C. **Figure 1e** and **Figure 1f** illustrate representative fluorescent images of the membrane and the measured filling ratio before and after the heating procedure. The average filling ratio before the heating was measured as 91.09%. Unfilled pores appeared to be random and likely caused by the sample's intermolecular forces overcoming the surface tension when the STAMP was removed from the glass. After 30 minutes

of heating at 37 °C, we observed evaporations in some parts of the membrane, where the filling ratio reduced to 83.54%. Those unfilled pores show no fluorescence signals and can be easily distinguished from those with negative reactions (which exhibit weak fluorescence signals, **Figure S2**). We did not observe partially filled pores under bright field microscope examination, likely due to the unfavorable surface tension conditions. To improve the accuracy of the absolute quantification, we only considered the filled pores as the total number of reactions in our system.

HIV-1 quantification principle and system characterization

After the development of the STAMP, we set out to develop a platform to utilize the STAMP for running the digital CRISPR (dCRISPR) assay for HIV-1 viral load quantification. The Cas13a reaction mix (~ 100 nL effective volume) was digitalized inside the membrane using the STAMP (**Figure 2a**). With binding to the specific RNA-guided target, Cas13a proteins become activated and perform trans-cleavage on the surrounding fluorophore-quencher (FQ) labeled single-stranded reporter [62] (**Figure 2b)**. Throughout the study, we utilized RNaseAlert substrate as our reporter, which is constructed by FAM dye linked with a quencher by single-stranded RNA [63].

Fluorescence images of the membranes were taken by a fluorescence microscope with a motorized stage to step through the whole membrane (**Figure 2c**). The light source wavelength was filtered to 480 nm using an excitation filter and redirected to the sample using a dichroic mirror. Afterward, the emitted light from the sample was obtained by CMOS camera after filtration at 535 nm. Twenty-four images were taken and stitched together to cover the whole membrane area (**Figure 2d**). The acquired images were analyzed to distinguish positive from negative pores based on the fluorescent intensity emitted from each pore. We utilized a *k*-means clustering algorithm to differentiate between positive and negative pores [64] (**Figure 2e and Figure S3**).

The Poisson statistics were utilized to quantify the number of HIV-1 RNA targets without external references. With *n* total number of filled pores, the positive pore ratio (*PPR*) is defined as *PPR=m/n*, where *m* is the number of positive reactions. Based on the Poisson statistics, the concentration of the RNA sample in the Cas13a reaction mix could be estimated as:

$$C = \frac{\lambda}{V_p} = -\frac{\ln(1-PPR)}{V_p} \quad (1)$$

where λ is the expected number of RNAs in each pore, and V_p is the average volume of the pores. After obtaining the RNA concentration in the Cas13a reaction mix, one can back-calculate the input RNA concentration.

We examined multiple no-target controls (NTC) to examine the background noise of STAMP-dCRISPR. **Figure 2f** presents the fluorescent images of the 4 NTC cases. While no targets were added in these cases, few positive pores were detected (**Table S1**). Multiple factors could cause the background noise in our systems, such as non-specific reporter cleavage [65-66], imaging hardware [67-68], and post-processing inaccuracy [67]. The system background noise, defined as $\mu_{NTC}+3\sigma_{NTC,}$ was determined to be 0.00093, where μ_{NTC} and σ_{NTC} are the averages and standard deviation of the *PPR* in the negative cases measured.

Design and optimization of HIV-1 Cas13 assay

To optimize the Cas13 crRNA design, we designed five crRNAs along the HIV-1 genome (red rectangles in **Figure 3a**, **Table S2**). In addition, we synthesized five 100 nucleotides target to cover each designed crRNA (colored rectangles in **Figure 3a**, **Table S3**). We cross-react the crRNAs with target samples and no target samples in a total of 30 reactions to validate the assay specificity. **Figure 3b** shows the fluorescent intensity over 60 minutes of Cas13a reactions. An increase in fluorescent intensity was only observed in cases where targets and crRNAs were matched, confirming the assay specificity. In the case of crRNA 3, no significant fluorescent signal increase was observed, likely due to the low or no trans-cleavage activity [33]. In addition, crRNA1 and 4 showed the highest trans-cleavage activity among the cases where the higher fluorescent intensity was observed after 60 minutes of reaction.

To further compare the performance of the Cas13a assay using crRNA 1 and 4, we performed a Michaelis-Menten kinetic study on the system. **Figure 3c** presents the measurements of reaction rates for the trans-cleavage activity of Cas13a proteins for crRNA1 and 4. Each data point is a measured initial reaction velocity (nM/s) for a titrated reporter concentration. **Figure S4** shows the details of cleaved reporter concentration and measurements of cleavage speed. To extract the kinetic properties of Cas13 proteins using crRNA1 and 4, the curves in **Figure 3d** were fitted using nonlinear regression based on the Michaelis-Menten equation:

$$V = k_{cat}\, E_0 \frac{[S]}{K_M+[S]} \quad (2)$$

where E_0 is the target-activated Cas/13−cRNA complex concentration, $[S]$ is the reporter concentration, k_{cat} is the catalytic turnover rate of the enzyme, and K_M is the Michaelis constant. For the reaction using crRNA 1 and 4, we obtained the catalytic rate (k_{cat}) of 60.32 s^{-1} and 29.49 s^{-1}, and catalytic efficiency (k_{cat}/K_M) of 0.05 nM s^{-1} and 0.04 nM s^{-1}, respectively. The assay using

crRNA1 displayed a reaction with a higher cleavage rate. In addition, we also quantified the bulk assay limit of detection using crRNA 1 and 4. As shown in **Figure 3d**, HIV-1 Cas 13 assay using crRNA1 showed a better limit of detection of ~200 pM compared to ~1 nM when using crRNA4. Therefore, crRNA 1 was chosen for our digital assay in the following studies.

Optimizing HIV-1 STAMP-dCRISPR assay time

To obtain the optimal reaction time for the HIV-1 assay, we measured the *PPR* at different reaction times for the Cas13a assay containing 5 fM HIV-1 synthetic RNA in the reaction mixture. **Figure 4a** presents the fluorescence images at various reaction times. As the reaction time increased, more positive pores were observed in fluorescent images. This happened because more reporters would be degraded in the positive pores as the reaction time increases, resulting in more wells reaching fluorescent intensity above the sensor detection sensitivity. **Figures 4b** and **Figures 4c** show the corresponding fluorescent intensity (FI) of positive and negative pores and their distributions, respectively. These results confirmed our observation that more positive pores were detected as the reaction time increased. To quantify the effect of reaction time, *PPR* was plotted from 0 to 60 minutes of reaction (**Figures 4d** and **Table S4**). As expected, the *PPR* increases as time passes; however, the ratio plateaus after 30 minutes. This means that the shortest time to develop a reliable *PPR* reading is about 30 minutes in our assay.

Based on the measured k_{cat} (**Figure 3c)**, a single activated Cas13a enzyme would produce ~13 nM of cleaved reporters (fluorescent probes) inside each pore (volume of 13 pL) in a 30-minute reaction. In contrast, a bulk reaction of 20 μL volume would only have produced ~ 9 fM cleaved reporters with the same 30 min reaction. Decreasing the reaction volume from microliter to picolitre would increase the fluorescent concentration by around 6 orders of magnitude and thus help improve the lower limit of detection.

Analytical performance test with synthetic HIV-1 RNAs

A series of synthetic HIV-1 RNA dilutions from 100 aM to 50 pM were tested to examine the quantitative analytical performance of the STAMP-dCRISPR. In each test, 2 μL of the synthetic target was used to form 20 μL of the reaction mixture, about 100 nL of which was loaded onto the membrane for analysis (see Methods: Digital Cas 13a assay with synthetic HIV-1 RNAs).

Figure 5a presents the fluorescent images at different synthetic RNA concentrations. As

expected, more positive pores were detected as RNA concentration increased. The *PPR* at different target concentrations is plotted in **Figure 5b**. Expectedly, the measured *PPR* increased from 3.7×10^{-4} at 100 aM to 0.99 at 50 pM. **Figure 5c** presents the measured concentrations via STAMP-dCRISPR versus the input synthetic target concentration (**Table S5**). These results showed the synthetic RNA quantification dynamic range of STAMP-dCRISPR is from 1 fM to 10 pM (4 orders of magnitude). Since a single membrane takes about 100 nL of 20 µL reaction mixture (with 2 µL RNA template) for analysis, the effective volume of synthetic RNA template analyzed on the membrane is about 10 nL. The dynamic range from 1 fM to 10 pM corresponds to an average of 6 and 60k synthetic RNA molecules. The measured concentrations in the linear dynamic range agree very well with the expected concentrations (R^2=0.998), confirming the absolute quantification capability of the STAMP-dCRIPSR. With the background noise defined as $\mu_{NTC}+3\sigma_{NTC}$, the LOD of the STAMP-dCRIPSR was determined to be around 1 fM. As compared to the LOD of 200 pM in the bulk assay shown in **Figure 3d,** the STAMP-dCRIPSR improved the LOD by >5 orders of magnitude. This enhancement is expected because the reaction volume was reduced from 20 µL (bulk) to 13 pL (digital). The 1 fM LOD in STAMP-dCRIPSR showed that digitization of the assay could improve the lower detection limit significantly.

Plasma viral load resolution test with contrived plasma samples

To examine the capability of the STAMP-dCRIPSR in resolving plasma viral load variations, we prepared a series of contrived plasma samples by spiking HIV-1 viral particles into healthy plasma. The viral load of these contrived plasma samples ranges from 7143 copies/mL to 21429 copies/mL, with a step change of 3571 copies/mL. Healthy plasma was used as a negative control. Each viral load was prepared in triplicates. The viral RNAs were extracted from these mock plasma samples using a column-based extraction process before being quantified using STAMP-dCRISPR (see Methods). Briefly, with 140 µL of the contrived plasma samples, we obtained 10 µL eluted RNAs, which were all used to form a total of 20 µL Cas 13a reaction mixture. Note this is different from the synthetic RNA test, in which we used 2 µL of RNA templates. This is to partially minimize the subsampling issue as each membrane would take about 100 nL of 20 µL reaction mixture for quantification analysis (*i.e.,* 0.5% of the initial analyte was analyzed in a single membrane).

Figure 6a shows six representative fluorescent images from these end-to-end plasma tests. As

expected, more positive pores were observed as increasing the plasma viral load. **Figure 6b** shows the plasma viral load obtained by STAMP-dCRISPR versus the expected values (see **Table S6** for testing statistics). As shown, the measured plasma viral load agrees very well with the input viral loads (R^2=0.996), confirming the capability of the STAMP-dCRISPR system for the quantification of plasma samples end to end. In addition, the *p*-value obtained from the t-test in **Figure 6b** showed that STAMP-dCRISPR could differentiate the plasma viral load with a resolution of at least 3571 copies/mL at the 90% confidence level. This is equivalent to resolving 3 copies of HIV-1 RNAs in a single membrane.

Validation test with clinical plasma samples

To demonstrate the clinical utility of STAMP-dCRISPR, we tested 20 clinical HIV plasma samples using STAMP-dCRISPR. Like the contrived plasma sample test, 10 μL of the RNA template was obtained from 140 μL of the plasma sample through a column-based extraction process. A total of 20 μL Cas 13a reaction mixture was then prepared and about 100 nL of this mixture was loaded onto the membrane for analysis. To compare the STAMP-dCRISPR with RT-PCR, two identical RNA templates were tested with STAMP-dCRISPR and RT-PCR, respectively. It should be noted that the RT-PCR used all 10 μL of the RNA template while STAMP-dCRISPR used only an effective 50 nL of the RNA template in a single analysis (see Methods). **Figure 7a** shows the STAMP-dCRISPR images of all these 20 clinical plasma samples. **Figure 7b** presents the real-time RT-PCR results of these clinical samples (CS1-CS20) and six concentration references for quantification (R1-R6). The RT-PCR calibration curve is plotted in **Figure S5** where the C_t values showed a linear relationship with the reference concentrations. Both the STAMP-dCRISPR and RT-PCR testing statistics are summarized in **Table S7**.

For the qualitative analysis of the results, **Figure 7c** shows the scattering plot between the mean C_t values of RT-PCR results and *PPR* values measured by STAMP-dCRISPR. The *PPR* corresponded well with C_t values for all negative samples and high positive samples with C_t<32. However, for low positive samples with C_t>32, the *PPR* values obtained from the STAMP-dCRISPR are limited by the noise floor. Using a *PPR* value of 4.5×10^{-4} as the positive/negative threshold, we tabulate the qualitative results as the inset of **Figure 7c.** The calculated sensitivity is 60%, and the specificity is 100%. Although the STAMP-dCRISPR is not intended for qualitative tests, the less ideal sensitivity is primarily due to the subsampling error, which arises in all assays

that could not analyze the entire volume of samples [69]. Notably, the effective volumes used in the RT-PCR and STAMP-dCRISPR tests are 10 μL and 50 nL, respectively. As a result, the RT-PCR test here is not subject to the subsampling error, while STAMP-dCRISPR suffers from significant subsampling issues, with only 0.5% of the eluted RNA template being analyzed.

For the quantitative analysis of the viral load, **Figure 7d** shows the viral load measured from the STAMP-dCRISPR versus that measured from the RT-PCR. The correlation between these two methods is excellent for viral loads > 2000 copies/mL (high positive regions). However, for PCR negatives and low positives (< 2000 copies/mL), the STAMP-dCRISPR is limited by the subsampling error. The observed plasma viral load limit of detection in STAMP-dCRISPR is about 2000 copies/mL. These results indicate that although the limit of detection performance should be further improved, the current STAMP-dCRISPR can perform absolute quantification when the plasma viral load is above 2000 copies/mL, even with an effective 50 nL RNA template being analyzed. The results in **Figure 7d** suggested the clinical relevance of the STAMP-dCRISPR for HIV viral load testing.

DISCUSSION AND CONCLUSION

CRISPR-based diagnostics has expanded from molecular biology discoveries to multiple FDA-authorized COVID-19 tests in just a few years [11]. Digital CRISPR provides a promising next-generation CRISPR diagnostic platform [70], such as amplification and calibration-free quantification and single-nucleotide specificity [38, 45]. Here, we reported a STAMP method to digitalize the CRISPR-Cas13 assay for amplification-free and absolute quantification of HIV-1 viral RNAs. A commercial PCTE membrane that is widely available and inexpensive would enable its wide adoption. In addition, the user-friendly STAMP device offers a convenient platform for individuals lacking expertise in microfluidics to utilize these membranes effectively (**Table S8**).

We developed, validated, and optimized the HIV-1 Cas13 assay. We evaluated the analytical performances with synthetic RNAs. With a single membrane that partitions ~100 nL reaction mixture, we showed that RNA samples spanning 4 orders of dynamic range between 1 fM (~6 RNAs) to 10 pM (~60k RNAs) could be quantified as fast as 30 min. We also examined the end-to-end performances from RNA extraction to STAMP-dCRISPR quantification using 140 μL plasma samples. We showed the device can detect 3571 copies/mL viral load change at a 90%

confidence level. Finally, we evaluated the device using 140 μL of 20 patient plasma samples and benchmarked the performance with RT-PCR. The STAMP-dCRISPR results agree very well with RT-PCR for all negative and high positive samples with plasma viral load above 2000 copies/mL.

While the current STAMP-dCRISPR provides a simple and amplification-free platform for HIV viral load quantification, several aspects of the system could be further improved in future studies. First, due to the subsampling errors, the STAMP-dCRISPR is currently limited in detecting low positive samples with plasma viral load below 2000 copies/mL. The current platform could only sample 0.5% of the eluted RNA template for plasma viral load quantification. Further limit of detection improvement of STAMP-dCRISPR could be achieved by (1) increasing the starting plasma sample volume to increase the eluted RNA sample concentration, (2) reducing the volume of Cas 13 reaction mix, (3) preconcentration of the sample such as magnetic-bead based preconcentration [47], and (4) adopting multiple membranes to increase the effective sample volume to be tested. Second, the current membrane-filling process of STAMP is still manual. Therefore the filling process could be inconsistent from run to run. Devising an automatic system for filling the membrane would eliminate case-by-case variations and alleviate the hands-on time process of the system [47]. Third, in terms of dynamic range of the system, the current STAMP-dCRISPR utilized a single membrane containing ~ 10^4 pores with an average volume of 13 pL. Based on the Poisson statistics in Eq.1, the minimum and maximum detectable concentrations *in the reaction mixture* would be 9.58 aM and 1.21 pM, respectively. The STAMP-dCRISPR showed a dynamic range between 100 aM and 1 pM. While the upper limit of the obtained dynamic range was close to the theory, the background noise affected the lower limit. Further pore volume and number optimization could improve the LOD and the dynamic range of STAMP-dCRISPR.

METHODS

STAMP device fabrication

The PMMA holders were prepared by cutting the PMMA sheets with 1/8" thickness using a laser cutter machine (Universal Laser System). Two pieces of PMMA with the dimensions of 24×24 mm and 35×35 mm with inner circles of 11 and 13 mm were fabricated and attached using acrylic cement (United States Plastic Corporation, cat# 46872). To handle the track-etched polycarbonate membranes (Sterlitech Corporation, cat# PCT25025100), we utilized a vacuum pen (Pen-vac pro series V8910). The PVP layer of the membranes was removed by dipping the

membranes in 10% acetic acid for 30 min, followed by heating to 140 °C for 60 min in a vacuum oven. Afterward, the membrane was attached to the holder using adhesive tapes (70 µm thickness). We used mineral oil purchased from Sigma-Aldrich (cat# 69794-500ML) to seal the membrane.

Data acquisition and analysis

The fluorescent images were taken using an inverted fluorescent microscope (Nikon ECLIPSE Ti). The integration time was set as 6 s to image the membrane. To cover the whole membrane, a motorized stage (Prior OptiScan) with a programmable step size in the x and y direction was utilized, and 24 images were taken to cover the whole membrane area. A customized MATLAB code was developed to stitch these 24 images with the x and y coordinates to reconstruct the whole membrane image. Afterward, A customized MATLAB code was used to implement a *k*-means clustering algorithm to differentiate between positive and negative pores. **Figure S3** illustrates the workflow of the stitching and clustering algorithm for data analysis.

HIV-1 specific crRNA design and selection

The optimal protospacer length observed for Cas13a is 28 nucleotides along [71]. In addition, Abudayyeh et al. analyzed the flanking regions of protospacers and found that sequences starting with a G immediately after the 3' end of the protospacer were less effective relative to all other nucleotides (A, U, or C) [72]. Therefore, considering the protospacer-flanking site (PFS), 28 nucleotide crRNA protospacer sequences were designed by targeting the HIV-1 type B sequence downloaded from the NCBI website. In the next step, 496 complete HIV-1 sequences deposited in the NCBI server were downloaded on 9/14/2021. These sequences were aligned using SnapGene software to find the stable and conservative region. We then searched and designed crRNAs against the aligned sequence with more than 80% similarity and chose five matched crRNAs (**Table S1**). It should be mentioned that we used a previously validated sequence for the direct repeat region of the crRNA as follows: 5'-GAUUUAGACUACCCCAAAAACGAAGGGGACUAAAAC -3' [23]. The designed crRNAs were synthesized by Integrated DNA Technologies. The crRNAs were resuspended in pH 7.5 buffer and stored at -80 ºC. LwaCas13a proteins were purchased from MCLAB (cat# CAS13a-100). Cas13a and crRNA were mixed in 1×PBS to form the non-activated Cas13a/crRNA at room temperature for 20 min and stored at -80ºC.

Bulk Cas 13a assay with synthetic HIV-1 RNAs

For bulk Cas 13a assay with synthetic HIV-1 RNAs, the total reaction volume is 20 μL, which consists of 2 μL of 125 nM non-activated Cas13a/crRNA complex, 2 μL of the RNA target (various concentrations), 9.5 μL of water, 0.5 μL of 40,000 units/ml Murine RNase Inhibitor (New England Biolabs, cat# M0314S), 2 μL of 4 μM FQ-labeled reporter (RNaseAlert substrate from IDT, cat# 11-04-02-03), and 4 μL of a CRISPR buffer consisting of 20 mM HEPES-Na pH 6.8, 50 mM KCl, 5 mM $MgCl_2$, and 5% glycerol. Afterward, the mixed solution was incubated in a 384-well plate (ThermoFisher, cat# 142761) using a microplate reader (Tecan plate reader infinite 200 PRO) at 37ºC. The fluorescent signal was measured every 30 s. The excitation wavelength was set as 480 nm with a bandwidth of 9 nm, and the emission wavelength was set as 530 nm with a bandwidth of 20 nm. The gain was 110, and the integration time was 20 μs.

Digital Cas 13a assay with synthetic HIV-1 RNAs

For digital Cas 13a assay with synthetic HIV-1 RNAs, the total reaction volume is also 20 μL and the components of the mixture are the same as in the bulk Cas 13a assay above. However, to transfer this reaction mix into the STAMP device, only 8 μL of the reaction mix was dropped on top of a glass surface to avoid overflow when filling the STAMP device. Each STAMP device then takes ~ 100 nL of CRISPR mixture for quantification analysis (note a single membrane has ~1.3×10^4 pores and each pore volume is about 13 pL). The sealed STAMP device was then placed on top of a hot plate (Fisherbrand Isotemp Hot Plate) at 37 °C for different reaction times.

End-to-end digital Cas 13a assay with plasma samples

Contrived plasma sample. To prepare the contrived plasma sample, different copies (1000, 1500, 2000, 2500, and 3000) of HIV viral particles (Seraseq, cat# 0740-0004) were spiked into 140 μL of fresh healthy plasma (Research Blood Components) to form a plasma viral load of 7143, 10714, 14286, 17857, 21429 copies/ml. After mixing, the plasma samples were preserved at -80 °C before use.

Clinical plasma sample. Twenty plasma samples collected from different patients were obtained from Hershey Medical Center by an approved institutional review board (IRB) of Pennsylvania State University. All samples were coded to remove information associated with patient identifiers. For each test, 140 μL of the clinical plasma sample was used.

HIV-1 RNA extraction from plasma samples. To extract the viral RNA from plasma samples, a column-based RNA extraction kit from Qiagen (cat# 52904) was utilized. The procedure is optimized for plasma samples with a volume of 140 µL. The plasma sample was first lysed under the highly denaturing conditions provided by a viral lysis buffer. We added carrier RNA to the lysis buffer, which enhances the binding of viral RNA to the kit membrane and reduces the chance of viral RNA degradation. Afterward, the purification was carried out in 3 steps using a standard centrifuge (Eppendorf centrifuge 5425). We washed the sample using ethanol and 2 washing buffers provided by the kit. In the final stage, we used 10 µL of nuclease-free water (BioLabs, cat# 52904B1500S) as an elution buffer to obtain the extracted RNAs from the membrane.

Digital Cas 13a assay with plasma extracted HIV-1 RNAs. To minimize the subsampling issue, the whole volume of the 10 µL eluted RNAs were used to form the Cas 13a reaction mixture. The total reaction volume is 20 µL, which consists of 2 µL of 125 nM non-activated Cas13a/crRNA complex, 10 µL of the eluted RNAs, 0.5 µL of water, 0.5 µL of 40,000 units/ml Murine RNase Inhibitor (New England Biolabs, cat# M0314S), 2 µL of 4 µM FQ-labeled reporter (RNaseAlert substrate from IDT, cat# 11-04-02-03), and 4 µL of a CRISPR buffer consisting of 20 mM HEPES-Na pH 6.8, 50 mM KCl, 5 mM $MgCl_2$, and 5% glycerol. Each STAMP device then takes ~ 100 nL of this 20 µL CRISPR mixture for quantification analysis. The sealed STAMP device was incubated at 37 °C for 30 min.

RT-PCR assay with plasma extracted HIV-1 RNAs. We used a one-step, two-enzyme RT-PCR protocol for testing clinical samples. The reaction has a total volume of 20 µL, consisting of 5 µL TaqMan Fast Virus 1-Step Master Mix (cat# 4444432, Thermofisher), 1.2 µL forward primer (0.6 µM), 1.2 µL reverse primer (0.6 µM), 0.5 µL probe (0.25 µM), and the 10 µL extracted RNA templates as well as 2.1 µL PCR grade water. We used a previously validated HIV-1 RT-PCR primer set (Forward primer: 5'- CATGTTTTCAGCATTATCAGAAGGA -3', and Reverse primer: 5'- TGCTTGATGTCCCCCCACT -3') [73]. In addition, the probe was selected as 5'- FAM-CCACCCCACAAGATTTAAACACCATGCTAA-Q -3', where Q indicates a 6-Carboxytetramethylrhodamine group quencher conjugated through a linker arm nucleotide. The following thermal cycling sequences performed the RT-PCR: 50 ℃ for the first five minutes without repeating to reverse transcription reactions which convert HIV-1 RNA into cDNA, then 95℃ for 20 seconds without repeating to initiate amplification, followed by 46 cycles of amplification stage consisting of 3 seconds of 95 ℃ and 30 seconds of 60℃ thermal-cycling.

ASSOCIATED CONTENT

A pre-print version of this work is available [74].

The Supporting Information is available. Effect of the peeling-off stage on the excess sample removal process. Typical fluorescent signals from negative and positive reactions. Algorithm for acquiring the fluorescent intensity and stitching of the images. Cleavage velocity measurements using crRNA1 and 4. The total number of filled and positive pores and the measured *PPR* for 4 negative control cases.The measured C_t values using RT-PCR versus the target RNA copies. Detailed sequences of designed crRNAs and targets. Reaction time test results. Synthetic RNA sample test results. Contrived plasma sample test results. Clinical plasma sample test results. Comparison to existing technologies. Illustration video for the device operation (PDF).

AUTHOR INFORMATION

Corresponding Author

* Email: Weihua Guan (wzg111@psu.edu)

ORCID

Weihua Guan: 0000-0002-8435-9672

Author contributions

W.G. conceived the concept and supervised the study. R.N., X.L. and Y.J. designed the Cas13a assay. R.N, A.J.P, and Y.J. validated the Cas13a assay. R.N. performed the digital assay and analyzed the data. R.N. and T.L. designed and performed the RT-PCR. Y.Z., J. J. N., W. H. Greene collected and tested the clinical samples. W.G. and R.N. co-wrote the manuscript, with discussion from all authors.

NOTES

A provisional patent related to the technology described herein is filed. The authors declare no other competing interests.

ACKNOWLEDGMENTS

This work was partially supported by the National Institutes of Health (R61AI147419) and the National Science Foundation (1902503, 1912410, 2045169). Any opinions, findings, conclusions or recommendations expressed in this work are those of the authors and do not necessarily reflect the views of the National Science Foundation and National Institutes of Health.

FIGURES AND CAPTIONS

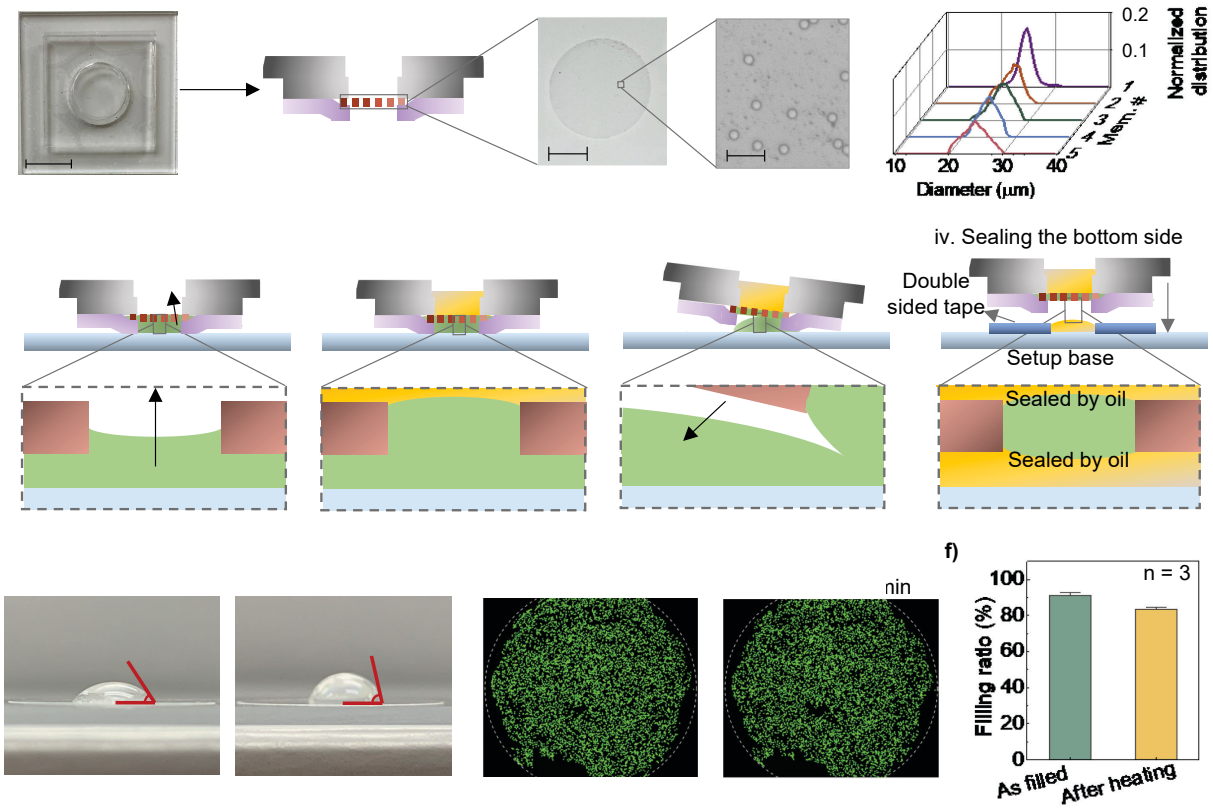

Figure 1. STAMP device characterization and filling process. a) Different components of the STAMP system, along with a top-side view of the assembled device and images of the commercial PCTE membranes. b) Pore size distribution of five different membranes and their total number of pores. c) STAMP process: **i.** The process starts by placing the STAMP on top of the sample. **ii.** The top side of the system is sealed by adding mineral oil. **iii.** STAMP is removed from the glass to eliminate the excess liquid from the bottom of the membrane. **iv.** STAMP is placed on the setup base (consisting of glass, double-sided tape, and mineral oil) to seal the bottom side of the system. d) Chemical treatment to remove the polyvinylpyrrolidone (PVP) coating from the PCTE membrane. The contact angle of a water droplet on top of the membrane increased from 48 to 79 degrees after treatment, confirming the effectiveness of the PVP removal process. e) Fluorescent images of a membrane demonstrating the filling of the membrane using STAMP before and after 30 minutes of heating at 37 °C. All filled pores are labeled with a filled green circle to demonstrate the filling process. f) Measured filling ratio of the membranes before and after 30 minutes of heating at 37 °C. We used a bright field image of the membrane to estimate the total number of pores. Afterward, the fluorescent image was used to count the filled pores. The error bar was defined as the 3×standard deviation of three replicates.

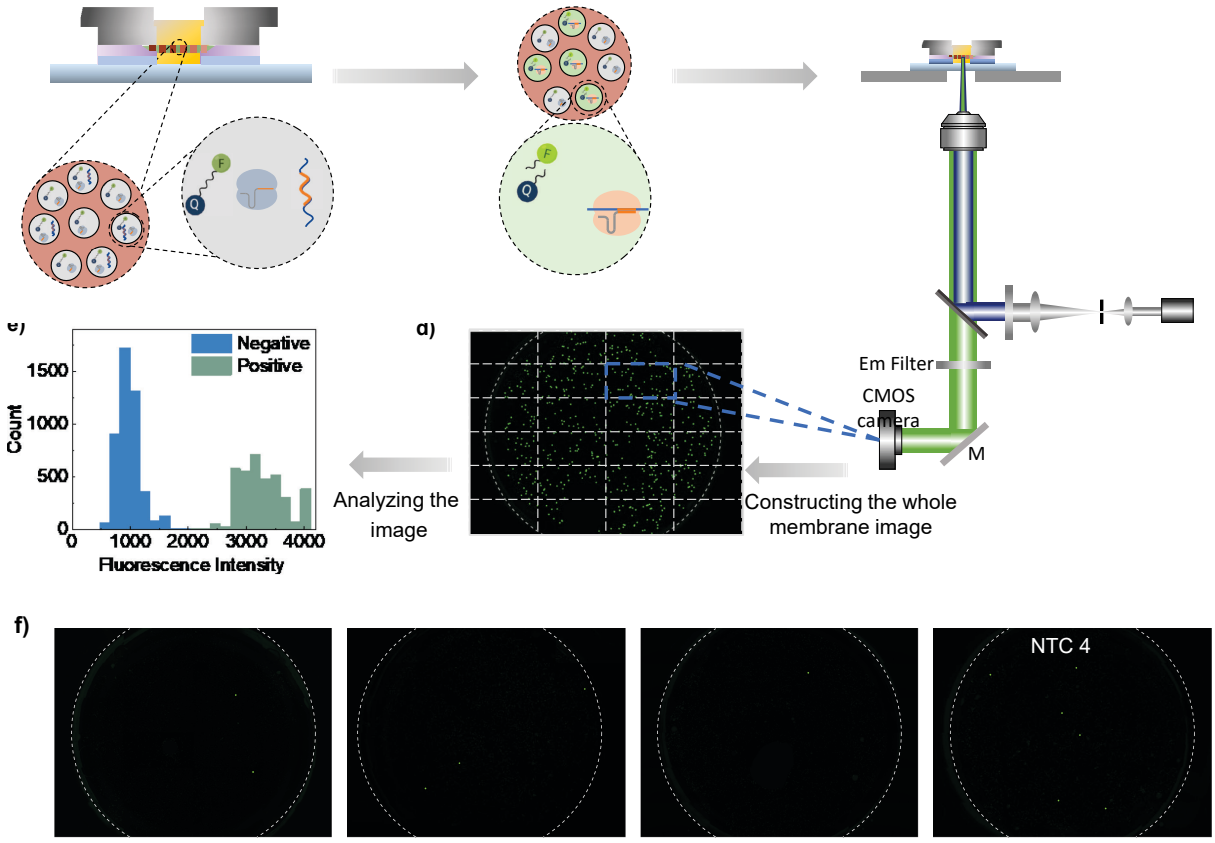

Figure 2. Utilization of STAMP device for running the digital CRISPR assay for HIV-1 viral load quantification. a) Digitization of CRISPR-Cas13a assay including HIV-1 RNA, Cas13a, and crRNA complex, fluorophore quencher (FQ)-labeled single-stranded RNA reporters. b) Trans-cleavage activity of the activated Cas13a proteins (after binding with HIV-1 RNAs) on non-target surrounding FQ RNA reporters. Cleavage of the reporters results in FAM fluorescence illumination. c) Fluorescent imaging setup. d) The fluorescent image of a whole membrane stitched from 24 images taken by the microscope. e) Clustering the positive and negative pores based on their fluorescent intensity using a k-means clustering algorithm. f) Fluorescent images illustrating positive and negative pores at 4 negative control cases. All positive pores are labeled with a filled green circle for better demonstration.

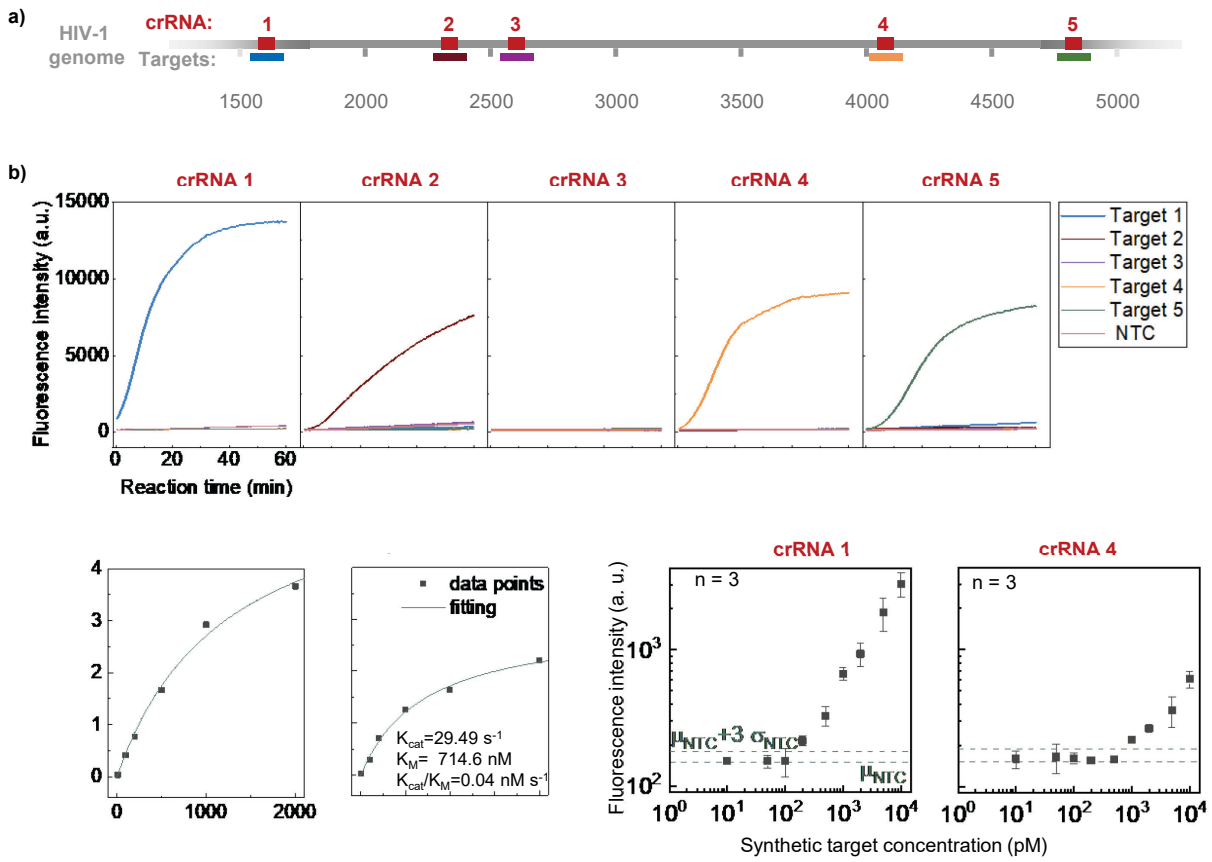

Figure 3. Optimization of Cas13 crRNA and bulk assay characterization. a) Schematic of the HIV-1 genome and the location of each crRNA spacer and the target region. b) Fluorescence intensity values over 60 minutes for 5 different crRNA and their corresponding targets (positive, 20 nM in 20 µL reaction), and no-target control (NTC) samples. c) Michaelis-Menten kinetic study of the Cas13a assay using crRNA 1 and crRNA 4. The RNA concentration is fixed at 20 nM in a 20 µL reaction. d) Sensitivity test of CRISPR assay using crRNA 1 and crRNA 4. In each case, three NTC cases were tested to determine the background fluorescent intensity as $\mu_{NTC}+3\sigma_{NTC}$, where μ_{NTC} and σ_{NTC} are the averages and standard deviation of the NTC cases, respectively. The error bar was defined as the 3×standard deviation of three replicates in each concentration.

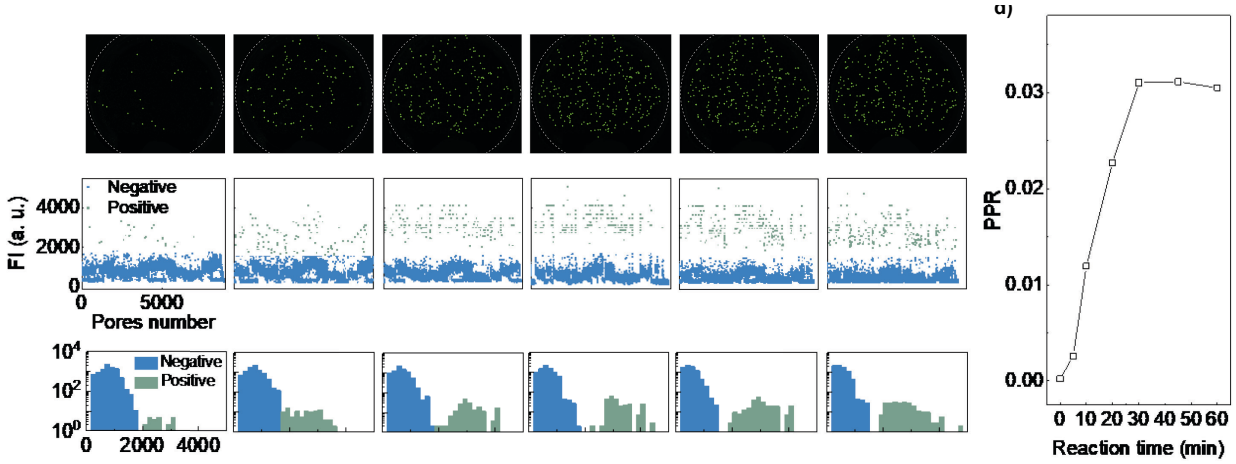

Figure 4. Optimizing STAMP-dCRISPR assay time. a) Fluorescent images illustrating the positive and negative pores at different reaction times from 0 to 60 minutes. The dashed grey circles illustrate the membrane edge. All positive pores are labeled with a filled green circle for better demonstration. b) Fluorescent intensity inside all filled pores (positive and negative) at different reaction times. Positive and negative pores are labeled as green and blue circles, respectively. c) Distribution of fluorescent intensity emitted from positive (green bars) and negative (blue bars) pores. d) The ratio of positive pores (*PPR*) at different reaction times.

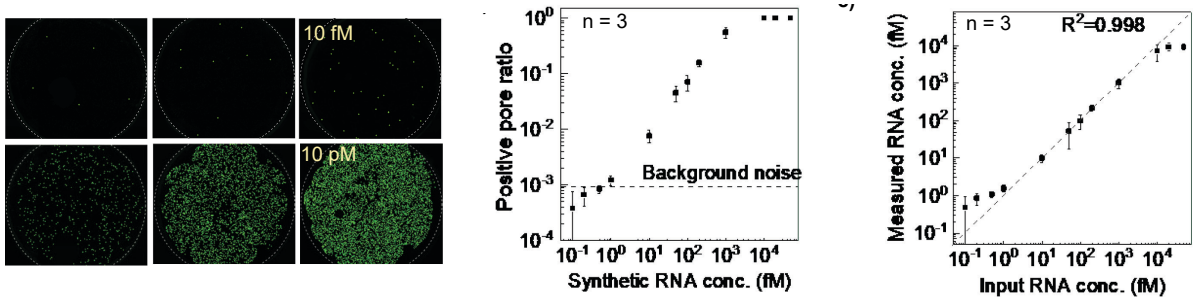

Figure 5. Analytical performance test using synthetic RNAs. a) Representative fluorescent images illustrating positive and negative pores at different synthetic RNA concentrations from 100 aM to 10 pM (2 µL RNA used in a total 20 µL reaction). All positive pores are labeled with a filled green circle for better visualization. b) The measured positive pore ratios (*PPR*) at different synthetic RNA concentrations from 100 aM to 50 pM. The dashed line represents the background noise. The error bar was defined as the 3×standard deviation of three replicates in each concentration. c) Comparison of measured synthetic RNA concentrations to the expected concentrations.

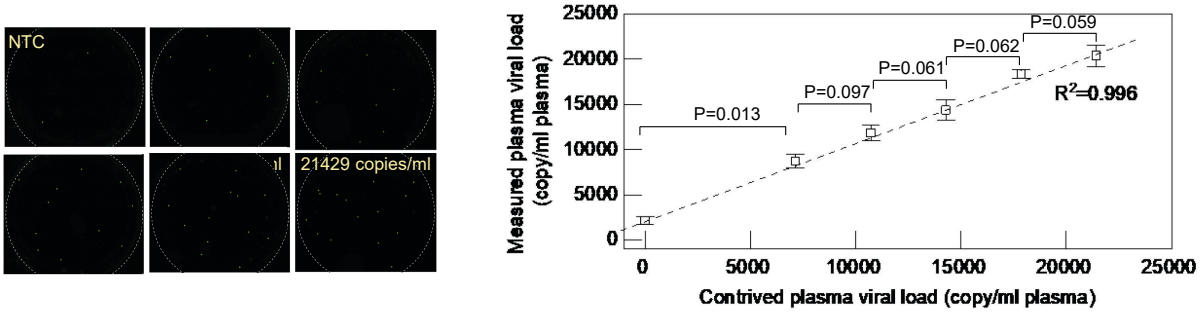

Figure 6. End-to-end viral load resolution test using contrived plasma sample. a) Representative fluorescent images obtained from testing the whole 10 µL extracted RNA template from 140 µL contrived samples. The total reaction mixture is 20 µL; about 100 nL was loaded on the membrane for analysis. All positive pores are labeled with a filled green circle for better visualization. b) Measured target concentration of the spiked samples along with the *p* values obtained from a t-test between adjacent cases.

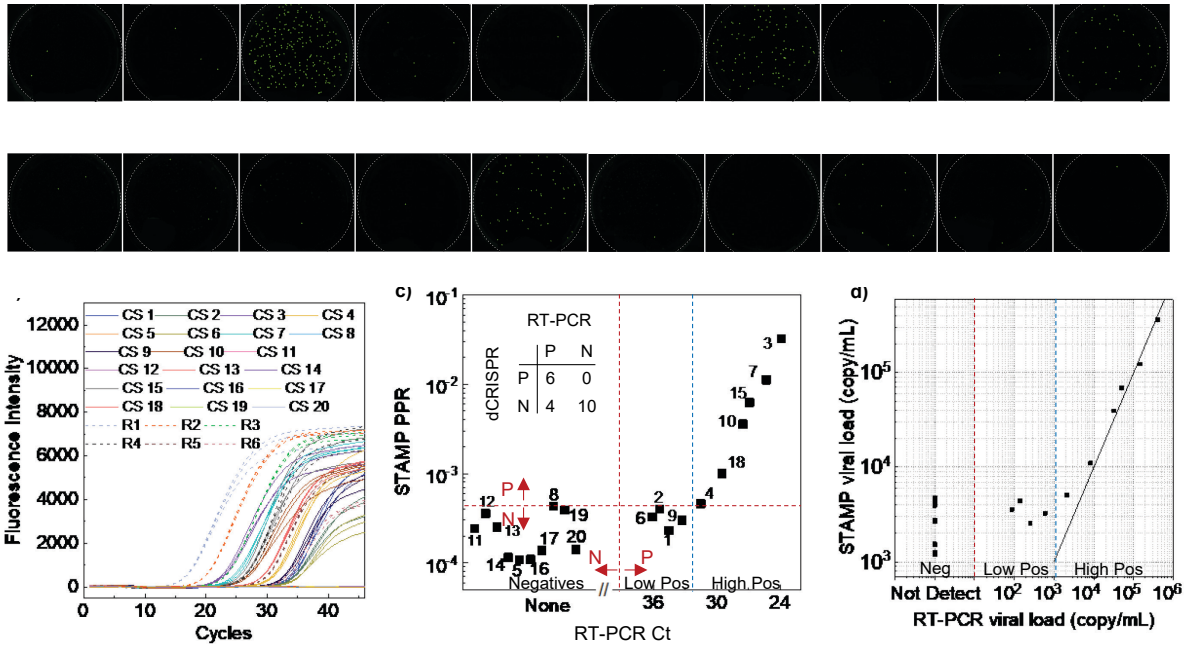

Figure 7. Clinical samples test using STAMP-dCRISPR. a) Fluorescent images illustrating positive and negative pores for clinical samples. The results were obtained using the total 10 µL extracted RNA template from 140 µL clinical samples. The total reaction mixture is 20 µL; about 100 nL was loaded on the membrane for analysis. All positive pores are labeled with a filled green circle for better demonstration. b) Real-time RT-PCR results for the clinical sample and the calibration references. c) Scattering plot between the mean C_t values of RT-PCR results and PPR values measured by STAMP-dCRISPR. The inset table summarizes the qualitative test results using 4.5×10^{-4} as the positive/negative threshold in STAMP-dCRISPR. (d) Viral load measured from the STAMP-dCRISPR versus that measured from the RT-PCR.

TOC

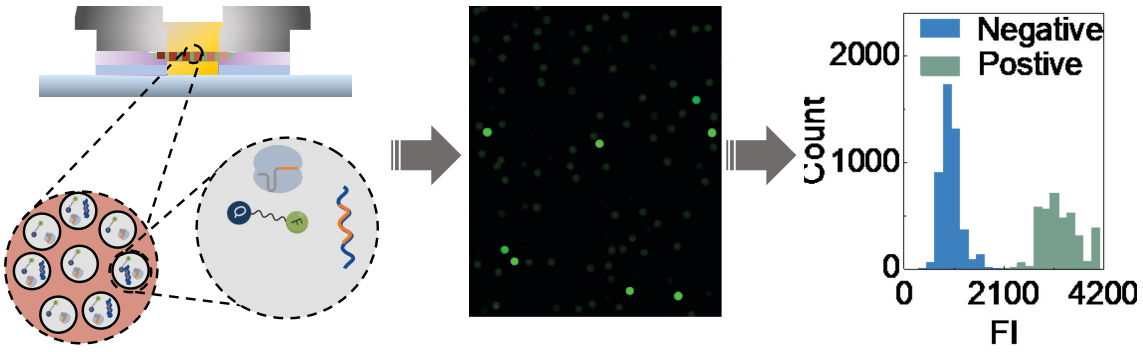

REFERENCE

1. Piot, P.; Bartos, M.; Ghys, P. D.; Walker, N.; Schwartländer, B., The global impact of HIV/AIDS. *Nature* **2001,** *410* (6831), 968-973.
2. UNAIDS. Global HIV & AIDS statistics - Fact sheet. https://www.unaids.org/en/resources/fact-sheet (accessed May 19, 2023).
3. Stekler, J. D.; Swenson, P. D.; Coombs, R. W.; Dragavon, J.; Thomas, K. K.; Brennan, C. A.; Devare, S. G.; Wood, R. W.; Golden, M. R., HIV testing in a high-incidence population: is antibody testing alone good enough? *Clinical infectious diseases* **2009,** *49* (3), 444-453.
4. Peter, J. B.; Sevall, J. S., Molecular-based methods for quantifying HIV viral load. *AIDS patient care and STDs* **2004,** *18* (2), 75-79.
5. Cobb, B. R.; Vaks, J. E.; Do, T.; Vilchez, R. A., Evolution in the sensitivity of quantitative HIV-1 viral load tests. *Journal of clinical virology* **2011,** *52*, S77-S82.
6. Saag, M. S.; Holodniy, M.; Kuritzkes, D.; O'Brien, W.; Coombs, R.; Poscher, M.; Jacobsen, D.; Shaw, G.; Richman, D.; Volberding, P., HIV viral load markers in clinical practice. *Nature medicine* **1996,** *2* (6), 625-629.
7. De Souza, M. S.; Phanuphak, N.; Pinyakorn, S.; Trichavaroj, R.; Pattanachaiwit, S.; Chomchey, N.; Fletcher, J. L.; Kroon, E. D.; Michael, N. L.; Phanuphak, P., Impact of nucleic acid testing relative to antigen/antibody combination immunoassay on the detection of acute HIV infection. *Aids* **2015,** *29* (7), 793-800.
8. Malnati, M. S.; Scarlatti, G.; Gatto, F.; Salvatori, F.; Cassina, G.; Rutigliano, T.; Volpi, R.; Lusso, P., A universal real-time PCR assay for the quantification of group-M HIV-1 proviral load. *Nature protocols* **2008,** *3* (7), 1240-1248.
9. Wang, S.; Xu, F.; Demirci, U., Advances in developing HIV-1 viral load assays for resource-limited settings. *Biotechnology advances* **2010,** *28* (6), 770-781.
10. Guichet, E.; Serrano, L.; Laurent, C.; Eymard-Duvernay, S.; Kuaban, C.; Vidal, L.; Delaporte, E.; Ngole, E. M.; Ayouba, A.; Peeters, M., Comparison of different nucleic acid preparation methods to improve specific HIV-1 RNA isolation for viral load testing on dried blood spots. *Journal of virological methods* **2018,** *251*, 75-79.
11. Abudayyeh, O. O.; Gootenberg, J. S., CRISPR diagnostics. *Science* **2021,** *372* (6545), 914-915.
12. Kaminski, M. M.; Abudayyeh, O. O.; Gootenberg, J. S.; Zhang, F.; Collins, J. J., CRISPR-based diagnostics. *Nature Biomedical Engineering* **2021,** *5* (7), 643-656.
13. Komor, A. C.; Badran, A. H.; Liu, D. R., CRISPR-based technologies for the manipulation of eukaryotic genomes. *Cell* **2017,** *168* (1-2), 20-36.
14. Li, S.-Y.; Cheng, Q.-X.; Wang, J.-M.; Li, X.-Y.; Zhang, Z.-L.; Gao, S.; Cao, R.-B.; Zhao, G.-P.; Wang, J., CRISPR-Cas12a-assisted nucleic acid detection. *Cell discovery* **2018,** *4* (1), 1-4.
15. Gootenberg, J. S.; Abudayyeh, O. O.; Lee, J. W.; Essletzbichler, P.; Dy, A. J.; Joung, J.; Verdine, V.; Donghia, N.; Daringer, N. M.; Freije, C. A., Nucleic acid detection with CRISPR-Cas13a/C2c2. *Science* **2017,** *356* (6336), 438-442.
16. Gootenberg, J. S.; Abudayyeh, O. O.; Kellner, M. J.; Joung, J.; Collins, J. J.; Zhang, F., Multiplexed and portable nucleic acid detection platform with Cas13, Cas12a, and Csm6. *Science* **2018,** *360* (6387), 439-444.
17. Abudayyeh, O. O.; Gootenberg, J. S.; Kellner, M. J.; Zhang, F., Nucleic acid detection of plant genes using CRISPR-Cas13. *The CRISPR Journal* **2019,** *2* (3), 165-171.
18. Li, S.-Y.; Cheng, Q.-X.; Liu, J.-K.; Nie, X.-Q.; Zhao, G.-P.; Wang, J., CRISPR-Cas12a has

both cis-and trans-cleavage activities on single-stranded DNA. *Cell research* **2018,** *28* (4), 491-493.
19. Bruch, R.; Baaske, J.; Chatelle, C.; Meirich, M.; Madlener, S.; Weber, W.; Dincer, C.; Urban, G. A., CRISPR/Cas13a‐powered electrochemical microfluidic biosensor for nucleic acid amplification‐free miRNA diagnostics. *Advanced materials* **2019,** *31* (51), 1905311.
20. Shao, N.; Han, X.; Song, Y.; Zhang, P.; Qin, L., CRISPR-Cas12a Coupled with Platinum Nanoreporter for Visual Quantification of SNVs on a Volumetric Bar-Chart Chip. *Analytical chemistry* **2019,** *91* (19), 12384-12391.
21. Li, L.; Li, S.; Wu, N.; Wu, J.; Wang, G.; Zhao, G.; Wang, J., HOLMESv2: a CRISPR-Cas12b-assisted platform for nucleic acid detection and DNA methylation quantitation. *ACS synthetic biology* **2019,** *8* (10), 2228-2237.
22. Qin, P.; Park, M.; Alfson, K. J.; Tamhankar, M.; Carrion, R.; Patterson, J. L.; Griffiths, A.; He, Q.; Yildiz, A.; Mathies, R., Rapid and fully microfluidic Ebola virus detection with CRISPR-Cas13a. *ACS sensors* **2019,** *4* (4), 1048-1054.
23. Kellner, M. J.; Koob, J. G.; Gootenberg, J. S.; Abudayyeh, O. O.; Zhang, F., SHERLOCK: nucleic acid detection with CRISPR nucleases. *Nature protocols* **2019,** *14* (10), 2986-3012.
24. Myhrvold, C.; Freije, C. A.; Gootenberg, J. S.; Abudayyeh, O. O.; Metsky, H. C.; Durbin, A. F.; Kellner, M. J.; Tan, A. L.; Paul, L. M.; Parham, L. A., Field-deployable viral diagnostics using CRISPR-Cas13. *Science* **2018,** *360* (6387), 444-448.
25. Dai, Y.; Somoza, R. A.; Wang, L.; Welter, J. F.; Li, Y.; Caplan, A. I.; Liu, C. C., Exploring the Trans‐Cleavage Activity of CRISPR‐Cas12a (cpf1) for the Development of a Universal Electrochemical Biosensor. *Angewandte Chemie* **2019,** *131* (48), 17560-17566.
26. Zhou, T.; Huang, R.; Huang, M.; Shen, J.; Shan, Y.; Xing, D., CRISPR/Cas13a powered portable electrochemiluminescence chip for ultrasensitive and specific MiRNA detection. *Advanced Science* **2020,** *7* (13), 1903661.
27. Nouri, R.; Jiang, Y.; Lian, X. L.; Guan, W., Sequence-specific recognition of HIV-1 DNA with solid-state CRISPR-Cas12a-assisted nanopores (SCAN). *ACS sensors* **2020,** *5* (5), 1273-1280.
28. Nouri, R.; Jiang, Y.; Tang, Z.; Lian, X. L.; Guan, W., Detection of SARS-CoV-2 with Solid-State CRISPR-Cas12a-Assisted Nanopores. *Nano letters* **2021,** *21* (19), 8393-8400.
29. Li, Y.; Li, S.; Wang, J.; Liu, G., CRISPR/Cas systems towards next-generation biosensing. *Trends in biotechnology* **2019,** *37* (7), 730-743.
30. Nouri, R.; Tang, Z.; Dong, M.; Liu, T.; Kshirsagar, A.; Guan, W., CRISPR-based detection of SARS-CoV-2: A review from sample to result. *Biosensors and Bioelectronics* **2021,** *178*, 113012.
31. Nouri, R.; Dong, M.; Politza, A. J.; Guan, W., Figure of Merit for CRISPR-Based Nucleic Acid-Sensing Systems: Improvement Strategies and Performance Comparison. *ACS sensors* **2022,** *7* (3), 900-911.
32. Ramachandran, A.; Santiago, J. G., CRISPR Enzyme Kinetics for Molecular Diagnostics. *Analytical Chemistry* **2021,** *93* (20), 7456–7464.
33. Fozouni, P.; Son, S.; de León Derby, M. D.; Knott, G. J.; Gray, C. N.; D'Ambrosio, M. V.; Zhao, C.; Switz, N. A.; Kumar, G. R.; Stephens, S. I., Amplification-free detection of SARS-CoV-2 with CRISPR-Cas13a and mobile phone microscopy. *Cell* **2021,** *184* (2), 323-333. e9.
34. Son, S.; Lyden, A.; Shu, J.; Stephens, S. I.; Fozouni, P.; Knott, G. J.; Smock, D. C.; Liu, T. Y.; Boehm, D.; Simoneau, C., Sensitive and multiplexed RNA detection with Cas13 droplets and kinetic barcoding. **2021**, 21261509. *MedRXiv*.

https://doi.org/10.1101/2021.08.02.21261509 (accessed May 19, 2023)
35. Zhang, L.; Zhang, K.; Liu, G.; Liu, M.; Liu, Y.; Li, J., Label-free nanopore proximity bioassay for platelet-derived growth factor detection. *Analytical chemistry* **2015,** *87* (11), 5677-5682.
36. Ding, X.; Yin, K.; Li, Z.; Sfeir, M. M.; Liu, C., Sensitive quantitative detection of SARS-CoV-2 in clinical samples using digital warm-start CRISPR assay. *Biosensors and Bioelectronics* **2021,** *184*, 113218.
37. Park, J. S.; Hsieh, K.; Chen, L.; Kaushik, A.; Trick, A. Y.; Wang, T. H., Digital CRISPR/Cas‐Assisted assay for rapid and sensitive detection of SARS‐CoV‐2. *Advanced Science* **2021,** *8* (5), 2003564.
38. Wu, X.; Tay, J. K.; Goh, C. K.; Chan, C.; Lee, Y. H.; Springs, S. L.; Loh, K. S.; Lu, T. K.; Yu, H., Digital CRISPR-based method for the rapid detection and absolute quantification of nucleic acids. *Biomaterials* **2021,** *274*, 120876.
39. Luo, X.; Xue, Y.; Ju, E.; Tao, Y.; Li, M.; Zhou, L.; Yang, C.; Zhou, J.; Wang, J., Digital CRISPR/Cas12b-based platform enabled absolute quantification of viral RNA. *Analytica Chimica Acta* **2022,** *1192*, 339336.
40. Yu, Z.; Xu, L.; Lyu, W.; Shen, F., Parallel Multistep Digital Analysis SlipChip Demonstrated with the Quantification of Nucleic Acid by Digital LAMP-CRISPR. *Lab on a Chip* **2022**.
41. Wu, X.; Chan, C.; Springs, S. L.; Lee, Y. H.; Lu, T. K.; Yu, H., A warm-start digital CRISPR/Cas-based method for the quantitative detection of nucleic acids. *Analytica Chimica Acta* **2022,** *1196*, 339494.
42. Liu, F. X.; Cui, J. Q.; Park, H.; Chan, K. W.; Leung, T.; Tang, B. Z.; Yao, S., Isothermal Background-Free Nucleic Acid Quantification by a One-Pot Cas13a Assay Using Droplet Microfluidics. *Analytical Chemistry* **2022,** *94* (15), 5883-5892.
43. Shinoda, H.; Taguchi, Y.; Nakagawa, R.; Makino, A.; Okazaki, S.; Nakano, M.; Muramoto, Y.; Takahashi, C.; Takahashi, I.; Ando, J., Amplification-free RNA detection with CRISPR–Cas13. *Communications biology* **2021,** *4* (1), 1-7.
44. Tian, T.; Shu, B.; Jiang, Y.; Ye, M.; Liu, L.; Guo, Z.; Han, Z.; Wang, Z.; Zhou, X., An ultralocalized Cas13a assay enables universal and nucleic acid amplification-free single-molecule RNA diagnostics. *ACS nano* **2020,** *15* (1), 1167-1178.
45. Yue, H.; Shu, B.; Tian, T.; Xiong, E.; Huang, M.; Zhu, D.; Sun, J.; Liu, Q.; Wang, S.; Li, Y., Droplet Cas12a assay enables DNA quantification from unamplified samples at the single-molecule level. *Nano Letters* **2021,** *21* (11), 4643-4653.
46. Yu, T.; Zhang, S.; Matei, R.; Marx, W.; Beisel, C. L.; Wei, Q., Coupling smartphone and CRISPR–Cas12a for digital and multiplexed nucleic acid detection. *AIChE Journal* **2021,** *67* (12), e17365.
47. Shinoda, H.; Iida, T.; Makino, A.; Yoshimura, M.; Ishikawa, J.; Ando, J.; Murai, K.; Sugiyama, K.; Muramoto, Y.; Nakano, M., Automated amplification-free digital RNA detection platform for rapid and sensitive SARS-CoV-2 diagnosis. *Communications Biology* **2022,** *5* (1), 1-8.
48. Lin, X.; Hu, X.; Bai, Z.; He, Q.; Chen, H.; Yan, Y.; Ding, Z., A microfluidic chip capable of switching W/O droplets to vertical laminar flow for electrochemical detection of droplet contents. *Analytica chimica acta* **2014,** *828*, 70-79.
49. Novak, R.; Zeng, Y.; Shuga, J.; Venugopalan, G.; Fletcher, D. A.; Smith, M. T.; Mathies, R. A., Single‐cell multiplex gene detection and sequencing with microfluidically generated agarose emulsions. *Angewandte Chemie International Edition* **2011,** *50* (2), 390-395.
50. Ma, Y.-D.; Luo, K.; Chang, W.-H.; Lee, G.-B., A microfluidic chip capable of generating and

trapping emulsion droplets for digital loop-mediated isothermal amplification analysis. *Lab on a Chip* **2018,** *18* (2), 296-303.
51. Schuler, F.; Trotter, M.; Geltman, M.; Schwemmer, F.; Wadle, S.; Domínguez-Garrido, E.; López, M.; Cervera-Acedo, C.; Santibáñez, P.; von Stetten, F., Digital droplet PCR on disk. *Lab on a Chip* **2016,** *16* (1), 208-216.
52. Yeh, E.-C.; Fu, C.-C.; Hu, L.; Thakur, R.; Feng, J.; Lee, L. P., Self-powered integrated microfluidic point-of-care low-cost enabling (SIMPLE) chip. *Science advances* **2017,** *3* (3), e1501645.
53. Zhu, Q.; Xu, Y.; Qiu, L.; Ma, C.; Yu, B.; Song, Q.; Jin, W.; Jin, Q.; Liu, J.; Mu, Y., A scalable self-priming fractal branching microchannel net chip for digital PCR. *Lab on a Chip* **2017,** *17* (9), 1655-1665.
54. Men, Y.; Fu, Y.; Chen, Z.; Sims, P. A.; Greenleaf, W. J.; Huang, Y., Digital polymerase chain reaction in an array of femtoliter polydimethylsiloxane microreactors. *Analytical chemistry* **2012,** *84* (10), 4262-4266.
55. Sun, B.; Shen, F.; McCalla, S. E.; Kreutz, J. E.; Karymov, M. A.; Ismagilov, R. F., Mechanistic evaluation of the pros and cons of digital RT-LAMP for HIV-1 viral load quantification on a microfluidic device and improved efficiency via a two-step digital protocol. *Analytical chemistry* **2013,** *85* (3), 1540-1546.
56. Bao, L.; Rezk, A. R.; Yeo, L. Y.; Zhang, X., Highly ordered arrays of femtoliter surface droplets. *small* **2015,** *11* (37), 4850-4855.
57. Yen, T. M.; Zhang, T.; Chen, P.-W.; Ku, T.-H.; Chiu, Y.-J.; Lian, I.; Lo, Y.-H., Self-Assembled Pico-Liter Droplet Microarray for Ultrasensitive Nucleic Acid Quantification. *ACS nano* **2015,** *9* (11), 10655-10663.
58. Gansen, A.; Herrick, A. M.; Dimov, I. K.; Lee, L. P.; Chiu, D. T., Digital LAMP in a sample self-digitization (SD) chip. *Lab on a Chip* **2012,** *12* (12), 2247-2254.
59. Rolando, J. C.; Jue, E.; Schoepp, N. G.; Ismagilov, R. F., Real-time, digital LAMP with commercial microfluidic chips reveals the interplay of efficiency, speed, and background amplification as a function of reaction temperature and time. *Analytical chemistry* **2018,** *91* (1), 1034-1042.
60. Lin, X.; Huang, X.; Urmann, K.; Xie, X.; Hoffmann, M. R., Digital loop-mediated isothermal amplification on a commercial membrane. *ACS sensors* **2019,** *4* (1), 242-249.
61. Lin, X.; Huang, X.; Zhu, Y.; Urmann, K.; Xie, X.; Hoffmann, M. R., Asymmetric membrane for digital detection of single bacteria in milliliters of complex water samples. *ACS nano* **2018,** *12* (10), 10281-10290.
62. Abudayyeh, O. O.; Gootenberg, J. S.; Essletzbichler, P.; Han, S.; Joung, J.; Belanto, J. J.; Verdine, V.; Cox, D. B.; Kellner, M. J.; Regev, A., RNA targeting with CRISPR–Cas13. *Nature* **2017,** *550* (7675), 280-284.
63. Patchsung, M.; Jantarug, K.; Pattama, A.; Aphicho, K.; Suraritdechachai, S.; Meesawat, P.; Sappakhaw, K.; Leelahakorn, N.; Ruenkam, T.; Wongsatit, T.; Athipanyasilp, N.; Eiamthong, B.; Lakkanasirorat, B.; Phoodokmai, T.; Niljianskul, N.; Pakotiprapha, D.; Chanarat, S.; Homchan, A.; Tinikul, R.; Kamutira, P.; Phiwkaow, K.; Soithongcharoen, S.; Kantiwiriyawanitch, C.; Pongsupasa, V.; Trisrivirat, D.; Jaroensuk, J.; Wongnate, T.; Maenpuen, S.; Chaiyen, P.; Kamnerdnakta, S.; Swangsri, J.; Chuthapisith, S.; Sirivatanauksorn, Y.; Chaimayo, C.; Sutthent, R.; Kantakamalakul, W.; Joung, J.; Ladha, A.; Jin, X.; Gootenberg, J. S.; Abudayyeh, O. O.; Zhang, F.; Horthongkham, N.; Uttamapinant, C., Clinical validation of a Cas13-based assay for the detection of SARS-CoV-2 RNA. *Nat*

Biomed Eng **2020,** *4* (12), 1140-1149.
64. Ortega, J. P.; Del, M.; Rojas, R. B.; Somodevilla, M. J. In *Research issues on k-means algorithm: An experimental trial using matlab*, CEUR workshop proceedings: semantic web and new technologies, 2009; pp 83-96.
65. Ono, T.; Ichiki, T.; Noji, H., Digital enzyme assay using attoliter droplet array. *Analyst* **2018,** *143* (20), 4923-4929.
66. Hunter, M. E.; Dorazio, R. M.; Butterfield, J. S.; Meigs‐Friend, G.; Nico, L. G.; Ferrante, J. A., Detection limits of quantitative and digital PCR assays and their influence in presence–absence surveys of environmental DNA. *Molecular ecology resources* **2017,** *17* (2), 221-229.
67. Milbury, C. A.; Zhong, Q.; Lin, J.; Williams, M.; Olson, J.; Link, D. R.; Hutchison, B., Determining lower limits of detection of digital PCR assays for cancer-related gene mutations. *Biomolecular detection and quantification* **2014,** *1* (1), 8-22.
68. Strain, M. C.; Lada, S. M.; Luong, T.; Rought, S. E.; Gianella, S.; Terry, V. H.; Spina, C. A.; Woelk, C. H.; Richman, D. D., Highly precise measurement of HIV DNA by droplet digital PCR. *PloS one* **2013,** *8* (4), e55943.
69. Basu, A. S., Digital assays part I: partitioning statistics and digital PCR. *SLAS technology* **2017,** *22* (4), 369-386.
70. Politza, A. J.; Nouri, R.; Guan, W., Digital CRISPR Systems for the Next Generation of Nucleic Acid Quantification. *Trends Analyt Chem* **2023,** *159*.
71. Khan, M. Z.; Amin, I.; Hameed, A.; Mansoor, S., CRISPR–Cas13a: prospects for plant virus resistance. *Trends in biotechnology* **2018,** *36* (12), 1207-1210.
72. Abudayyeh, O. O.; Gootenberg, J. S.; Konermann, S.; Joung, J.; Slaymaker, I. M.; Cox, D. B.; Shmakov, S.; Makarova, K. S.; Semenova, E.; Minakhin, L., C2c2 is a single-component programmable RNA-guided RNA-targeting CRISPR effector. *Science* **2016,** *353* (6299), aaf5573.
73. Palmer, S.; Wiegand, A. P.; Maldarelli, F.; Bazmi, H.; Mican, J. M.; Polis, M.; Dewar, R. L.; Planta, A.; Liu, S.; Metcalf, J. A., New real-time reverse transcriptase-initiated PCR assay with single-copy sensitivity for human immunodeficiency virus type 1 RNA in plasma. *Journal of clinical microbiology* **2003,** *41* (10), 4531-4536.
74. Nouri, R.; Jiang, Y.; Politza, A. J.; Liu, T.; Greene, W.; Nunez, J.; Lian, X. L.; Guan, W., STAMP-Based Digital CRISPR-Cas13a (STAMP-dCRISPR) for Amplification-Free Quantification of HIV-1 Plasma Viral Load. **2022,** 512138. *bioRxiv*. https://doi.org/10.1101/2022.10.13.512138 (accessed May 19, 2022)